Irrigation Science (2025) 43:87–103
https://doi.org/10.1007/s00271-024-00955-1

ORIGINAL PAPER

Thermal imaging from UAS for estimating crop water status in a Merlot vineyard in semi-arid conditions

Luz K. Atencia Payares[1,2,3] · Maria Gomez-del-Campo[1,2] · Ana M. Tarquis[1,4] · Mónica García[5]

Received: 4 January 2024 / Accepted: 14 July 2024 / Published online: 30 July 2024

Abstract

Thermal remote sensing indicators of crop water status can help to optimize irrigation across time and space. The Crop Water Stress Index (CWSI), calculated from thermal data, has been widely used in irrigation management as it has a proven association with evapotranspiration ratios. However, different approaches can be used to calculate the CWSI. The aim of this study is to identify the most robust method for estimating the CWSI in a commercial Merlot vineyard using high-resolution thermal imaging from Unoccupied Aerial Systems (UAS). To that end, three different methods were used to estimate the CWSI: Jackson's model (CWSIj), Wet Artificial Reference Surface (WARS) method (CWSIw), and the Bellvert approach (CWSIb). A simpler indicator calculated as the difference between canopy and air temperature (Tc–Ta) was the benchmark to beat. The water status of a vine cultivar with anisohydric behavior (Merlot) in a vineyard in central Spain was assessed for two years with different agroclimatic conditions. Canopy temperature (Tc) was obtained from UAS flights at 9:00 h and 12:00 h solar hour over eight days during the irrigation period (June–August), and from vines under five different irrigation treatments. Stem water potential (SWP), stomatal conductance (gs), and leaf temperature (TL) were recorded at the time of the flights and compared with the thermal indices (CWSIj, CWSIw, CWSIb) and the benchmark indicator (Tc–Ta). Results show that the simpler indicator of water stress, Tc–Ta, performed better at identifying varying levels of crop hydration than CWSIb or CWSIw at 12:00 h. Under conditions of extreme aridity, the latter indices were less accurate than the physically-based CWSIj at 12:00 h, which had the highest correlation with SWP ($r = 0.84$), followed by the benchmark index Tc–Ta ($r = 0.70$ at 12:00). Considering the current climatic trends towards aridification, the CWSIj emerges as a useful operational tool, with robust performance across days and times of day. These results are important for irrigation management and could contribute to improving water use efficiency in agriculture.

Keywords CWSI · UAS · Water stress · Thermography · Vineyard

Introduction

Given the ever-worsening impacts of climate change, the rational use of water resources is critical. However, this requires effective water management and decision-making under conditions of high uncertainty (FAO 2020). The situation is particularly acute in climate change hotspots, such as the semiarid central region of Spain, La Mancha, where irrigation accounts for around 80% of the consumptive use of water, leading to groundwater overexploitation (Closas et al. 2017).

Grapevines (*Vitis vinifera* L.) are one of Spain's key crops, and the third most important woody crop after olives and non-citrus fruit trees (Ministerio de Agricultura 2021). The surface area in Spain dedicated to grapevines

✉ Luz K. Atencia Payares
lkatenciapayares@gmail.com

1 CEIGRAM, ETSIAAB, Universidad Politécnica de Madrid (UPM), Senda del Rey St. 13, 28040 Madrid, Spain

2 Dpto. de Producción Agraria, ETSIAAB, Universidad Politécnica de Madrid (UPM), Ciudad Universitaria s.n, 28040 Madrid, Spain

3 Unmanned Technical Works (UTW), 28919 Leganés, Madrid, Spain

4 Grupo de Sistemas Complejos, ETSIAAB, Universidad Politécnica de Madrid (UPM), Ciudad Universitaria s.n, 28040 Madrid, Spain

5 Estación Experimental de Zonas Áridas (EEZA-CSIC), La Cañada de San Urbano s/n, 04120 Almería, Spain

for winemaking amounts to almost 1 million hectares (ha), with 30% of this area under irrigation.

In semiarid regions, vines are frequently exposed to drought stress (Costa et al. 2016; Van Leeuwen et al. 2018), impacting vegetative and reproductive growth, fruit composition, and wine quality (Van Leeuwen et al. 2018). The amount and timing of irrigation play a crucial role in achieving high yields and good quality fruit (Intrigliolo and Castel 2010). While mild or moderate water deficits generally enhance berry sugar and phenolic compound accumulation, severe water stress may significantly reduce berry quality (sugar, aroma) and grape yields (Leeuwen et al. 2009; Van Leeuwen et al. 2018). There is thus a need for effective irrigation planning based on adaptive management over time and space, with water allocation across sub-zones tailored to the specific water status of the vines.

Physiological parameters such as stem water potential (SWP) measured with pressure chambers (Scholander et al. 1965) or stomatal conductance (gs) measured with leaf diffusion porometers have been used to assess the water status of various crops (Hsiao 1990; Shackel et al. 1997). However, these methods are too time-consuming to allow for comprehensive field characterization. Hence, there is growing demand for new cost-effective technologies to assess spatial and temporal variability in the water status of vines (Fuentes et al. 2013; Romero et al. 2018).

Infrared thermography is widely used to monitor plant water status (Gates 1964; Jackson et al. 1977; Jones 1999, 2002; Jones et al. 2009) and plan irrigation scheduling (Jones 2004; Cohen et al. 2005, 2017; Meron et al. 2010). When transpiration decreases due to stomatal closure, leaf temperature increases with the decline in the evaporative cooling in the leaf. Therefore, thermal imagery is particularly suitable for monitoring the ratio of actual evapotranspiration (ET) to potential evapotranspiration (ETp), with the ratio ET/ETp often used as an indicator of crop water stress (Jackson et al. 1981; Gonzalez-Dugo et al. 2014; Nieto et al. 2022). A subsequent non-trivial step is relating the evapotranspiration ratio to changes in SWP or leaf water potential (LWP) (Möller et al. 2007; Berni et al. 2009; Bellvert et al. 2016) or canopy conductance (Gutiérrez et al. 2021).

Recently, thermal imaging has become more accessible to users at sub-meter resolutions, making it compatible with farm-scale applications using different platforms such as aircraft, balloons, mobile platforms, and Unoccupied Aerial Systems (UAS) (Berni et al. 2009; Wang et al. 2019). The use of UAS is of particular interest due to their potential as a tool for agricultural surveillance. UAS could complement satellite and aircraft imaging, and help overcome their shortcomings. For example, they could provide high-resolution near real-time imaging, with fewer challenges relating to fuel or piloting issues, enabling enhanced surveillance and improvements in decision-making (Rejeb et al. 2022).

The crop water stress index (CWSI) is one of the more popular indices for quantifying water stress using thermal remote sensing (Jackson et al. 1981; Berni et al. 2009). It has been identified as a good crop water status indicator and proposed as a possible substitute for SWP (Bellvert et al. 2020). CWSI can be calculated with a simple scaling operation, where the observed canopy temperature, Tc, is normalized by the Tc of a fully transpiring crop (Twet) and the Tc of a crop that is not transpiring at all (Tdry). However, it is a challenge to correctly estimate Twet and Tdry, and both theoretical (Jackson et al. 1981) and empirical approaches have been proposed for their estimation (Idso 1982). In the theoretical approach, Twet and Tdry are evaluated from a physically-based model such as Penman–Monteith and mass-transfer equations for the turbulent fluxes. This estimation requires micrometeorological information that is not always easy to obtain at a local level, such as wind speed, global radiation, or aerodynamic and stomatal resistances (Jackson et al. 1981). While there are other empirical approaches that may be simpler, they tend to be crop- and site-specific. Idso (1982) related the canopy–air temperature difference (Tc–Ta) of a canopy transpiring at a potential rate to the vapor pressure deficit (VPD). Other alternatives involve creating direct observations of Twet, e.g. by spraying leaves with soapy water on both sides to maintain their moisture or using a polystyrene float covered in wet fabric (Meron et al. 2003). To estimate Tdry, leaves can be covered with Vaseline on both sides to prevent transpiration (Jones 2002), or a rough approach involves adding 5 °C to the dry bulb temperature (Irmak et al. 2000). To develop operational information systems on crop water status, it is critical to find robust approaches that can be used to estimate Twet and Tdry over time and under various soil water conditions, avoiding in situ field measurements as much as possible.

The relationship between thermal indices and LWP or SWP presents another challenge. These parameters have long been used as the agronomic indicators of plant water status (Naor 2000; Choné et al. 2001; Girona et al. 2006). The CWSI has been empirically related to both of these, mostly on a day-to-day basis (Möller et al. 2007; Wheaton et al. 2011; Bellvert et al. 2014) as a strong dependency on the day and time of day is observed (Bellvert et al. 2014, 2015; Santesteban et al. 2017). It is not entirely clear whether the SWP-CWSI relationship holds across different multitemporal scenarios and plant water use strategies along the isohydricity continuum (Pou et al. 2012).

The aim of this study is to evaluate the potential of the CWSI, calculated using information from a thermal camera on board a UAS, to estimate grapevine water status at solar noon (12:00 h) and morning (9:00 h) in a commercial Merlot vineyard with predominantly anisohydric behavior (Williams and Baeza 2007). A key contribution of this study is that it provides evidence of the most readily operational

way to calculate a water stress indicator (CWSI) that can be used to estimate SWP.

As part of this analysis, we evaluated three methods for calculating the CWSI and establishing its robustness for estimating SWP and gs across different times of day. We chose Tc–Ta as the benchmark to beat. The three methods under evaluation are: the original method based on theoretical energy balance and the Penman–Monteith equation (Jackson et al. 1981; Berni et al. 2009); a method using artificial references (Möller et al. 2007); and the empirical method proposed by Idso et al. (1982) and adapted for different grapevine varieties by Bellvert et al. (2015).

Materials and methods

Site and vineyard description

The commercial vineyards are located in Yepes, Toledo (Spain) at 39°56′25.8" N 3°43′22.4" W (WGS84, UTM zone 30N), at an altitude of 570 m above sea level (masl) and covering an area of around 40 ha.

Twenty-year-old Merlot grapevines (*Vitis vinifera* L.) grafted on SO4 (Selection Oppenheim 4) rootstock are grown in the selected area. Vine rows are oriented northeast and arranged on a trellis with a plantation frame of 2.60 × 1.10 m. The study was conducted during the 2021–2022 irrigation seasons.

The site has a Mediterranean climate, with warm, dry summers and mild winters. The average daily temperature is 15.3 °C, average rainfall is low (338.4 mm) and evaporative demand is high (1350 mm).

Climatic and irrigation conditions

Daily shortwave radiation, Rs (MJm^{-2}), air temperature (°C), wind speed (ms^{-1}), rainfall (mm), and reference evapotranspiration, ETo (mm) data were obtained from a meteorological station in Magán, Toledo (Toledo: 505 masl, Latitude: 40° 2′ 5.81″N Longitude: 3° 20′ 3.49″W), located 13 km from the experimental zone.

The meteorological conditions are presented in Fig. 1. Annual rainfall was similar in 2021 and 2022, registering a value of 349 and 348 mm, respectively. Rainfall between January and May was 167 mm in 2021 and 173 mm in 2022. The corresponding values during the experimental period (June–August) were 36 mm in 2021 and 2 mm in 2022. Differences in annual ETo were observed, with values of 1284 mm in 2021 and 1395 mm in 2022. The ETo from January to May was 416 mm in 2021 and 804 mm in 2022. The conditions were highly evaporative during the experimental period (June–August) with high cumulative ETo (390 and 441 mm in 2021 and 2022, respectively). In short, 2022 was drier than 2021, resulting in a higher evaporative demand.

Regarding temperature, August was the hottest month in 2021 (Tmean 27.5 °C), and July was the hottest in 2022 (Tmean 29.8 °C).

Irrigation was applied from May 17 to August 27, 2021, and from June 23 to September 01, 2022. The irrigation treatments are described in Table 1. The number of drippers was adjusted for each treatment to achieve different irrigation doses, from T100, T50, T25 and T0 refer to different doses of surface irrigation: T100 (reference treatment), T50 (50% of reference treatment), T25 (25% of reference treatment), and T0 (rainfed). T25-S, refers to subsurface irrigation (25% of reference treatment). The drippers had an

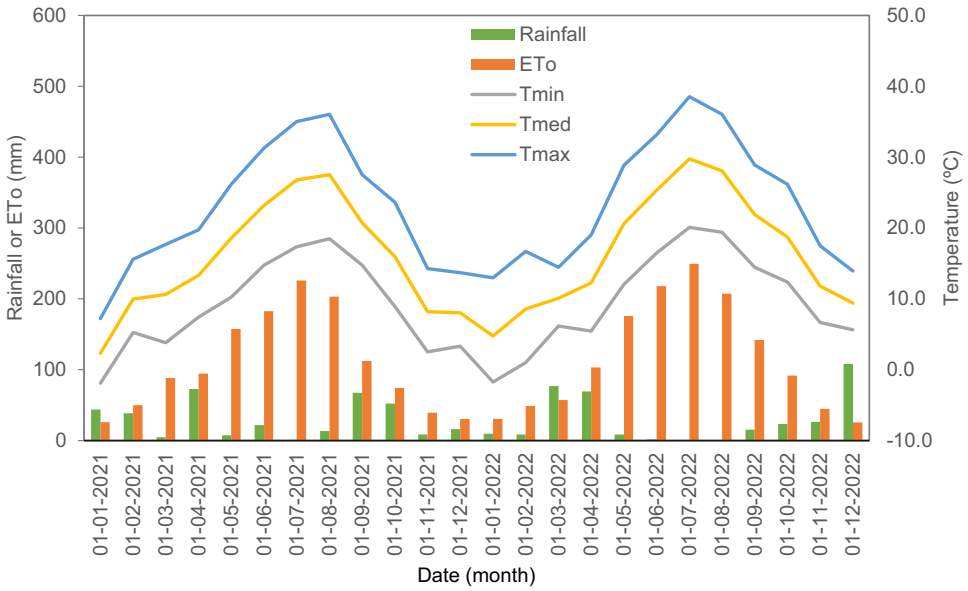

Fig. 1 Monthly rainfall (Rainfall), reference evapotranspiration (ETo), and minimum (Tmin), average (Tmean) and maximum (Tmax) temperatures from October 2020 to September 2022. The data were recorded by the weather station located in Magán (Toledo, Spain) (adapted from Atencia Payares et al. 2023)

Table 1 Description of the five irrigation treatments

Treatment	N° drippers/plant	System	Doses 2021 (mm/year)	Doses 2022 (mm/year)
T100	4	Surface	428.0	258.7
T50	2	Surface	214.0	129.4
T25	1	Surface	107.0	64.7
T25-S	1	Subsurface	107.0	64.7
T0	none	Surface	rainfed	rainfed

T100 (reference treatment), T50 (50% of reference treatment), T25 (25% of reference treatment), T0 (rainfed) and T25-S (25% of reference treatment applied subsurface). Treatments applied over the two years of the study in the experimental vineyard (Toledo, Spain)

application rate of 2 l h^{-1}. A 40% reduction in irrigation occurred in the second year due to farm-level management of drought conditions. This was in response to an increase in the costs, bearing in mind that it is a commercial farm.

During the 2021 irrigation season, there were a total of 154 h of watering, distributed in daily 3 h sessions. In 2022, there were 93 h of watering, distributed in daily 2 h sessions. The irrigation was scheduled from Monday to Friday in both years.

Field data collection

For this study, we obtained meteorological information from a portable weather station. This information included measurements of air temperature within the canopy (Ta), and relative humidity, RH (%) to calculate vapor pressure deficit (VPD). In addition, the portable weather station recorded temperature information from a wet artificial reference surface (WARS) between the hours of 9:00 h and 12:00 h (solar time). The WARS consisted of a wet, non-woven fabric covering a polystyrene float. The float was placed in a 0.28×0.3 m water-filled plastic box, and the fabric was kept constantly wet. The thermocouple air temperature and relative humidity sensor were connected to a data logger. Average values were recorded every minute.

SWP (MPa) was assessed on healthy mature leaves in the shade and enclosed for 1 h in aluminum foil bags to reach the water status equilibrium between leaf and stem. SWP was measured using a Scholander pressure chamber (Soil Moisture Equipment Corp., Santa Barbara, CA, USA). The leaf stomatal conductance (mmol m^{-2} s^{-1}) was measured with a portable gas exchange system CIRAS2 (PP Systems, Hitchin, Hertfordshire, UK). We refer to the leaf stomatal conductance measured this way as gs.

SWP and gs were measured on six vines per irrigation treatment. Measurements were all conducted simultaneously with the UAS image acquisition.

UAS image acquisition and processing

Eight UAS flight campaigns were carried out at the vineyard site during different weather conditions in 2021 and 2022 at 9:00 h and 12:00 h (Table 2). The UAS surveys were conducted at 120 m above ground level.

The eBee SenseFly fixed-wing UAS platform, equipped with a Duet-T sensor (AgEagle Aerial Systems Inc. Wichita, Kansas), was used to collect thermal data. The thermal sensor included a high-resolution thermal infrared camera and a senseFly SODA RGB camera.

Data from the multispectral camera (Parrot Sequoia) were used to obtain the normalized difference vegetation index (NDVI) and subsequently calculate the simple ratio vegetation index (see Annex II).

The experimental vines were identified in the image using QGIS 3.4 software (QGIS, Free Software Foundation, Boston, MA, USA), following a similar protocol to the one described in Atencia Payares et al. (2023). Each canopy vine was demarcated, and 30 regions of interest (one per plant) of 0.30×0.30 m were extracted, avoiding pixels with shadows and soil. A total of five pixels per vine were obtained with the thermal camera. The very high spatial resolution made

Table 2 Information on multispectral and thermal sensors

Dates	Camera	Acquisition time (h)	Spectrum (nm)	SR (m/pixel)	Overlap	Purpose
June 25 2021 July 05 2021 July 20 2021 July 30 2021	Parrot Sequoia Multispectral	9:00 12:00	G (530–570) R (640–680) Redge (730–740) NIR (770–810)	0.14	70%	NDVI
June 30 2022 July 15 2022 August 05 2022 August 12 2022	Duet-T	9:00 12:00	Thermal infrared (FLIR) 700-1200nm	0.16	80%	Tc

G green, *R* red, *Redge* red edge, *NIR* near-infrared, *SR* spatial resolution, *NDVI* normalized difference vegetation index, *Tc* canopy temperature and the dates they were used

it possible to distinguish between leaves and soil and the selected pixels that contained sunlit leaves.

Temperature correction

Thermal imagery radiometric and atmospheric corrections were processed as indicated in Annex I. For the post-processing of the radiometric temperature data, we followed the methodology proposed Wang et al. (2019), obtaining land surface temperature by removing atmospheric effects using a single-channel atmospheric correction.

At-sensor radiometric temperature (Ts) was converted to surface temperature (Tc) through atmospheric and emissivity corrections.

Once the images had been radiometrically corrected, we extracted Tc from the pixels of the vines where SWP was measured. We manually selected the pixels in each vine to ensure that only pure crown vegetative pixels were taken. This information was taken each day of the UAS flight campaign.

Crop water stress index

Three different method were used to determine the Twet and Tdry from the CWSI.

Bellvert method

The empirical approach to estimate the wet and dry baselines proposed by Idso (1982) was adapted by Bellvert et al. (2015) for grapevines based on phenological state and variety. The lower and upper baselines (Tdry and Twet) are estimated as a function of VPD.

Based on Bellvert et al. (2015), we considered the Tdry or upper limit and Twet or lower limit from the Tempranillo cultivar, which shows similar anisohydric behavior to the Merlot cultivar (Williams and Baeza 2007). We selected the equations from Stage II-III, where Stage II is from fruit-set to veraison; and Stage III is from veraison to harvest.

$$Twet = Tc - Ta = -1.780VPD + 1.253 \quad (1)$$

$$Tdry = Tc - Ta = 0.446VPD + 5.317 \quad (2)$$

where (Tc–Ta) is in °C, and VPD is in KPa.

Jackson's energy balance method

Analytical approaches seek to address uncertainties arising from dry and wet conditions by integrating surface energy balance fluxes such as net radiation (R_n), sensible heat (H), and latent heat (λE). The baselines are estimated using the energy balance and Penman–Monteith equations. For our study, we used an updated version of the methodology presented by Jackson et al. (1981, 1982), which considered VPD, wind speed, differences in net radiation, and crop resistances. This approach does not require reference surfaces and relies on physical models to estimate all input variables of the energy balance and mass-transfer equations.

The surface energy balance equation is:

$$R_n - G = H + \lambda E \quad (3)$$

where R_n is the net radiation (W m^{-2}), G is the heat flux below the canopy (W m^{-2}), H is the sensible heat flux (W m^{-2}) from the canopy to the air, and λE is the latent heat flux to the air (W m^{-2}), with λ being the heat of vaporization (Jackson et al. 1981) A starting assumption of the model is that pure vegetation Tc can be retrieved from thermal imagery if the spatial resolution allows pure crown pixels to be distinguished from sunlit and shadowed soil pixels.

In our study, we selected only pixels of vegetation, therefore G is likely to be negligible. The fact that the resolution of Tc is very high means this issue is less important than when bare soil is present in the estimates, as the energy stored in the foliage can be considered negligible (Schymanski et al. 2013).

Assuming that the energy stored in the foliage and the energy used in the photosynthetic processes are negligible (Berni et al. 2009), the energy balance in the canopy foliage is written as:

$$R_n = H_c + \lambda E_c \quad (4)$$

where R_n is the net radiation (Wm^{-2}), H_c is the sensible heat flux into the air (Wm^{-2}), and λE_c is the latent heat flux (Wm^{-2}). The subscript c denotes that only the canopy energy fluxes are considered.

The terms H_c and λE_c can be expressed as:

$$H_c = \rho C_p \frac{(T_c - T_a)}{r_a} \quad (5)$$

$$\lambda E_c = \frac{\rho C_p (e_c^* - e_a)}{\lambda (r_a + r_c)} \quad (6)$$

where ρ is the air density (kg m^{-3}); C_p is the specific heat of the air (J kg^{-1} °C); Tc and Ta are, respectively, the temperature of the canopy (°C) and of the air (°C); r_a is the aerodynamic resistance (s m^{-1}); e_c^* is the saturated vapor pressure (Pa) at the canopy temperature;e_a is the actual vapor pressure of the air (Pa); γ the psychrometric constant (Pa $°C^{-1}$); and r_c is the canopy resistance to vapor transport (s m^{-1}).

Combining Eqs. (4), (5) and (6) r_c (sm^{-1}) is calculated as:

$$r_c = \frac{r_a\left(e_c^* - e_a\right)}{\gamma\left(\frac{r_a R_n}{\rho C_p} - \left(T_C - T_a\right)\right)} - r_a \quad (7)$$

To solve this equation, Ta and e_a can be retrieved from a portable weather station, whereas ρC_p and γ are calculated from Ta and atmospheric pressure. Tc can be measured using thermal imagery acquired from thermal infrared sensors.

Following Moyano et al. (2018), R_n (Wm^{-2}) has to be modeled to obtain the Rn-daily (see Annex II).

The following equation was used to calculate r_a:

$$r_a = \frac{ln(\frac{SH-Z*0.67}{Z*0.123}) * ln\frac{SH-Z*0.67}{Z*0.0123}}{k^2 * U} \quad (8)$$

where U is the wind speed (ms^{-1}) (Allen et al., 1994), and SH and k are, respectively, the sensor reference height (2 m above the canopy) and the Von Karman constant (0.4). Z*0.67, Z*0.123 and Z*0.0123 are the zero displacement height (m), the roughness length momentum (m) and the roughness length for sensible heat exchange (m), respectively (Maes and Steppe 2012).

An analytical solution for the CWSI can be obtained once r_c and the potential canopy resistance for a non-water stressed crop (r_{cp}) are known (Jackson 1982).

$$CWSI = 1 - \frac{ET}{ET_p} = \frac{\gamma\left(1 + \frac{r_c}{r_a}\right) - \gamma *}{\Delta + \gamma(1 + \frac{r_c}{r_a})} \quad (9)$$

where Δ is the slope of the saturation vapor pressure vs temperature regression and:

$$\gamma *= \gamma(1 + r_{cp}/r_a) \quad (10)$$

r_{cp} estimates have been published for many crops and can be estimated on the basis of stomatal conductance values (Bota et al. 2016; Toro et al. 2019). For our study, we obtained an empirical value from a portable gas exchange system, CIRAS-2 (PP Systems, Hitchin, Hertfordshire, UK). To estimate the parameter, we used the mean maximum gs found for the full irrigation treatment as an estimate of the potential resistance, which falls within the range of values reported in previous studies on vineyards.

Wet artificial reference surface (WARS) method

This method for estimating baselines involves the use of natural (Clawson et al. 1989; Leinonen and Jones 2004) or artificial (Meron et al. 2003) wet and dry reference surfaces. Examples have been reported for Merlot (Möller et al. 2007) and Cabernet Sauvignon (Wheaton et al. 2011).

This method is the simplest for calculating the CWSI but requires in situ measurements.

In our study, to estimate Twet, we used polystyrene foam as a permanently wet surface of reproducible physical properties, as detailed by Cohen et al. (2005). Tdry was estimated by adding 5°C to the measured dry bulb temperature (Irmak et al. 2000).

The CWSI was calculated (Jones and Corlett 1992) as follows:

$$CWSI = \frac{T_{canopy} - T_{wet}}{T_{dry} - T_{wet}} \quad (11)$$

where Tc is the actual canopy temperature obtained from the thermal image, and Twet was taken as the average temperature of the WARS.

Indicators estimated for model validation

To compare the robustness of the different indices, we have included estimated three parameters: gsmodel(TL), gsmodel(Tc), and CWSIj(TL). The first two refers to conductance (gs) estimated using the Jackson model with leaf temperature (TL) and canopy temperature (Tc), respectively. CWSIj(TL) is calculated using TL values instead of Tc values.

An analysis of variance (ANOVA) was applied to the different variables using Infostat version 1.5 (National University, Córdoba, Argentina). The means were separated using the LSD-test (< 0.05) for statistical differences. Spearman test was applied to assess the relationship between stem water potential (SWP) and thermal indices, moreover, Spearman correlation matrix were calculated to assess the relationship between mean physiological and thermal-based remote sensing indices, using free R studio statistical software (RStudio Inc. Boston, Massachusetts, United States).

Results

Weather conditions within the canopy

Table 3 shows the differences in Ta, RH, and VPD within the canopy between the two times of day at which the measurements and image were obtained.

As expected, Ta was lower at 9:00 h than at 12:00 h, RH decreased over the course of the day to 12:00 h, and VPD was higher at 12:00 h than at 9:00 h. If we compare the average of these dates in 2021 and 2022 for all the variables, Ta increased from 30.4 at 9:00 h to 35 °C at 12:00 h in 2021 and from 31.1 to 36.7 °C in 2022. Therefore, the temperature was 1 °C higher at 9:00 h and 12:00 h in 2022 than at the same times in 2021. RH was 39% lower at 9:00 and 22% lower at

Table 3 Air temperature (Ta), relative humidity (RH), and vapor pressure deficit (VPD) within the canopy during the days of the UAS flight at 9:00 and 12:00 h

Dates	9:00 h			12:00 h			ETo (mm/day)
	Ta (°C)	RH (%)	VPD(KPa)	Ta (°C)	RH (%)	VPD(KPa)	
June 25 2021	29.0	39.3	2.4	33.5	29.7	3.6	6.6
July 05 2021	29.8	39.7	2.5	35.0	29.0	4.0	8.2
July 20 2021	30.8	33.9	2.9	37.5	18.5	5.3	7.9
July 30 2021	32.0	15.9	4.0	34.1	10.8	4.8	9.1
AVERAGE 2021	**30.4**	**32.2**	**3.0**	**35.0**	**22.0**	**4.4**	**7.9**
June 30 2022	27.6	27.6	2.7	30	23.1	3.3	7.0
July 15 2022	35.1	22.5	4.4	41.3	14.2	6.8	8.1
August 05 2022	31.2	34.4	3.0	37.9	18.2	5.4	7.3
August 12 2022	30.6	28.5	3.1	37.4	21.2	5.0	6.3
AVERAGE 2022	**31.1**	**28.3**	**3.3**	**36.7**	**19.2**	**5.1**	**7.2**

Values in bold correspond to the average of the dates for each year

Daily reference evapotranspiration (ETo) for the reference crop according to FAO56 Penman–Monteith (1998) of the same date. Values in bold correspond to the average of the dates for each year.

12:00 in 2022 compared to 2021. Concerning VPD, higher differences between the years were found at 12:00 h than at 9:00 h. In both years, VPD was around 3 kPa at 9:00 h.

However, we obtain more information if we quantify the differences on each date in each year. The first three dates in 2021 show a positive trend in Ta, with the increases between 9:00 h to 12:00 h going from + 4.5 °C to + 6.7 °C, whereas on the last date (July 30, 2021) the increase was just + 2.1 °C. This relatively smaller increase is due to the fact that the temperature was already high in the morning on that date. On the contrary, in 2022, the first date shows an increase in Ta of only + 2.1 °C, with increases of around + 6.5 °C on the rest of the dates. These values reflect the fact that the 2022 season began with high temperatures in the morning.

RH shows a clear decrease from one year to the next. At 9:00 h, it was 39% lower in 2022 than at the same time in 2021, and at 12:00 h, it was 22% lower in 2022 than in 2021.

The differences in VPD in 2021 show the same pattern as those in Ta and RH. In the case of 2022, the middle dates show a VPD difference of + 2.4 kPa, with the first and last dates registering differences of + 0.6 and + 1.9 kPa, respectively.

Effect of irrigation treatment on physiological parameters

The SWP values ranged from − 0.43 MPa for T100 (9:00, July 5 2021) to − 1.80 MPa for T0 (12:00, August 12 2022), with a marked reduction in SWP values in all treatments in the drier year (2022) compared to the previous year (2021), especially at 9:00 h. For instance, the T100 average values in 2022 were 106% lower than in 2021 at 9:00 h, and 73% lower at 12:00 h.

SWP was lower at 12:00 h (Fig. 2b) than at 9:00 h (Fig. 2a), but differences between morning and noon were higher (41%) in 2021 compared to the drier and hotter 2022 (16%). The effect of soil water deficit was apparent in the annual average SWP, which was significantly higher in T100 compared to T25, T25-S and T0.

The effect of irrigation levels on water status was more evident in 2021 than in 2022. The rainfed treatment (T0) shows higher variability at noon than the other treatments.

The response of gs to irrigation levels was similar to that of SWP (Fig. 2c,d), with lower mean values in the hotter and drier year (2022), especially at noon. The maximum gs value (222 mmol/m^2s^2) was recorded on June 25, 2021, at 9:00 h and the minimum at the end of the dry year on August 5 2022 at 12:00 h (17 mmol/m^2s^2. The reduction in gs between 2021 and 2022 for the maximum irrigation level (T100) was 61% and 50% at 9:00 and 12:00 h, respectively. The T25-S presented the smallest reduction compared to the other treatments at both times of day.

The gs value was lower at 12:00 h than at 9:00 h, but differences were higher (44%) in 2021 compared to 2022 (19%). In 2022, the gs values were already low in the morning. Significant differences in gs between the irrigation treatments were observed in both years. The annual average gs was significantly higher in T100 compared to the other treatments. Furthermore, T25, T0, and T25-S did not present significant differences in most measurements.

Figure 2 (e and f) shows the TL of leaves exposed to the sun, measured manually with the gas exchange equipment

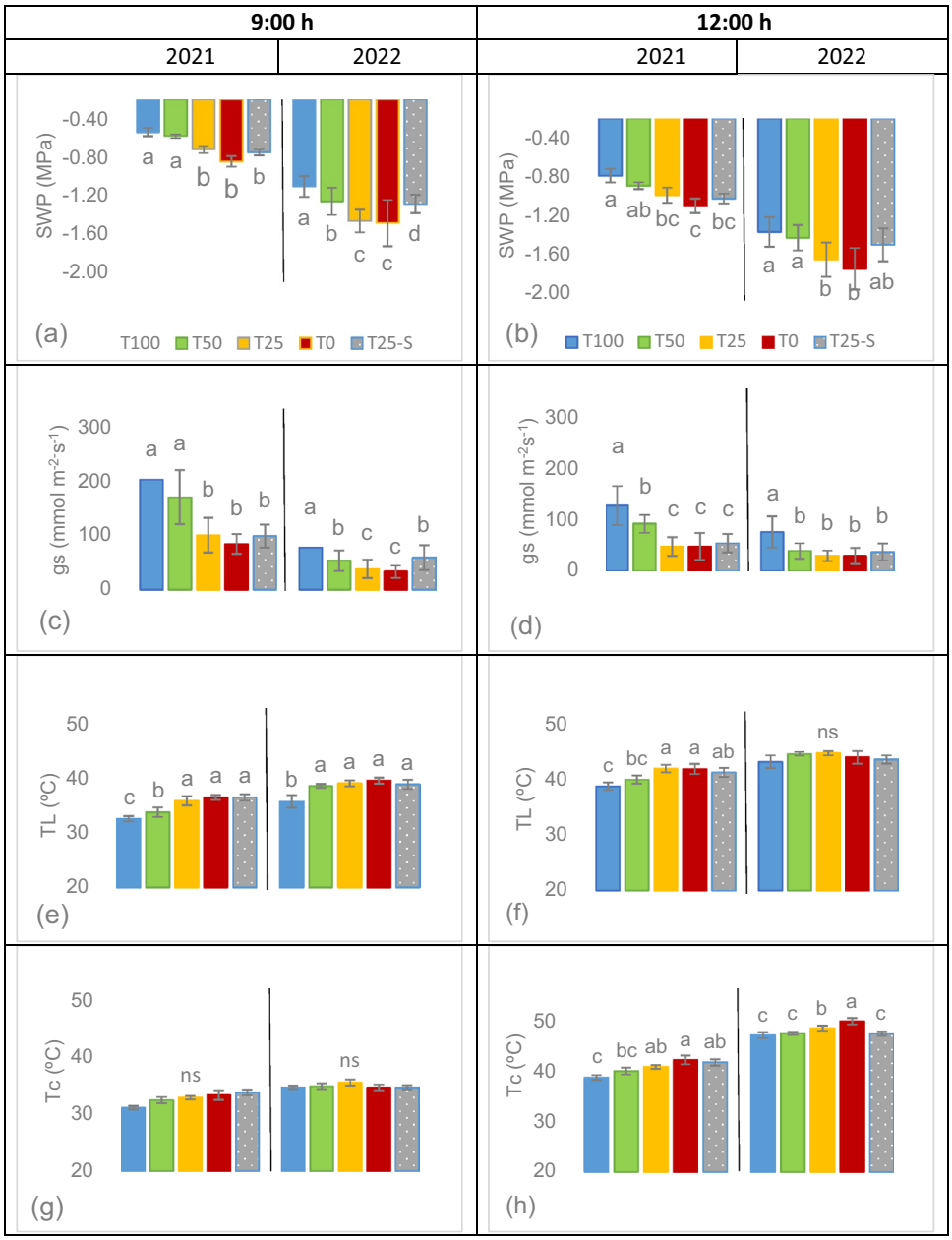

Fig. 2 measurement dates average Stem water potential (SWP., MPa) (**a**,**b**), Stomatal conductance (gs)(**c**,**d**) Temperature Leaf (TL)(**e**,**f**), Temperature canopy (Tc) (**g**,**h**) at 9:00 and 12:00 h in both years (2021, 2022) by irrigation treatments: T100 (reference treatment), T50 (50% of reference treatment), T25 (25% of reference treatment), T0 (rainfed) and T25-S (25% of reference treatment applied subsurface)

CIRAS2. The average values ranged from 31.4 (9:00 h June 25, 2021) to 46 °C (12:00 h August 5, 2022). The TL was higher in 2022 than in 2021. In 2022, TL in T100 was 2.8 and 1.7 °C higher than in 2021 at 9:00 h and 12:00 h, respectively. The annual average TL in 2021 was 6 °C higher at 12:00 h than at 9:00 h in treatment T100.

The irrigation treatment significantly affected the TL, especially in 2021 at 9:00 h. For both years, the annual average TL at 9:00 h was significantly lower in T100 than in the other treatments. Specifically, T100 was 4 °C lower than T0 at 9:00 h in both years. Significant differences were not observed for T25, T0, and T25-S in most measurements and values.

The Tc estimated by a thermal camera on board UAS is shown in Fig. 2 (g, h). The values ranged from 27.5 (9:00 h, June 25, 2021) to 51.2 °C (12:00 h, July 15, 2022). The average increase in Tc for all the treatments in 2022 was 2 and 7 °C higher than in 2021 at 9:00 h and 12:00 h, respectively. In 2022, Tc in T100 was 3.5 and 8 °C higher than in 2021 at 9:00 h and 12:00 h, respectively.

Regarding the two measures of temperature, the TL presented significant differences between treatments at both 9:00 h and 12:00 h in 2021. However, in 2022, significant differences between treatments were observed only in the early morning. Conversely, the Tc values obtained by the drone did not reveal differences between treatments at the

9:00 h measurement; however, they were more sensitive at the 12:00 h measurement.

Tc, the radiometric temperature, mainly reflecting the top of the canopy longwave emission, was significantly related to TL (TL = 1.36*Tc–15.52, R^2 = 0.74). Tc was lower than TL for values of TL below 43 °C but similar to TL at values above 43 °C.

This relationship explains the similarity in average temperatures at solar noon between the two parameters in 2021, with values of 40.6 and 40.8 °C for Tc and TL, respectively.

Relationship between SWP and gs

Significant nonlinear relationships were observed between gs and SWP at 9:00 h (Fig. 3a) and 12:00 h (Fig. 3b). At 9:00 h, values of gs decreased rapidly until − 0.57 MPa and then more gradually as SWP increased. However, the behavior observed at 12:00 h was not as clear, showing more dispersion.

Observations at 9:00 h showed a change in trend at − 0.57 MPa with an R^2 of 0.54. At 12:00 h, the breakpoint occurred at − 0.88 with an R^2 of 0.36. To determine where this breakpoint occurred, we used a piecewise function.

At 9:00 h, the following equations were obtained:

if SWP < = − 0.57 y = 161.58 + 79.88*(SWP), if SWP > − 0.57 y = 161.58 + 79.88*(− 0.568) + (79.88 + 83 6.38) *(SWP-(− 0.57)).

The potential of thermal indices to estimate water status

Linear regressions between SWP and thermal indices were used to evaluate the potential usefulness of these indices for estimating the water status of the vines. All the thermal indices performed better at 12:00 h than at 9:00 h. Of all the indices, the CWSIj at 12:00 h had the most significant correlation with SWP (r = 0.84) (Fig. 4d). It was followed by the benchmark index Tc–Ta (r = 0.70 at 12:00 h) (Fig. 4b), while the other two indices—CWSIw (Fig. 4f) and CWSIb (Fig. 4h)—performed worse, with similar values of r at 12:00 h (0.64 and 0.63, respectively).

Some values are observed to deviate from the linear relationship present at 12:00 h for all indices: these values occurred on July 30 2021 (solid red circle). The solid black circles correspond to the rest of the measurement dates in 2021. The open black circles correspond to measurement dates in 2022.

A Spearman correlation matrix was calculated between all the indices and the physiological parameters (gs and SWP). Figure 5 visualizes all the possible positive and negative relationships between the measured and estimated indices, and their strength of these relationship.

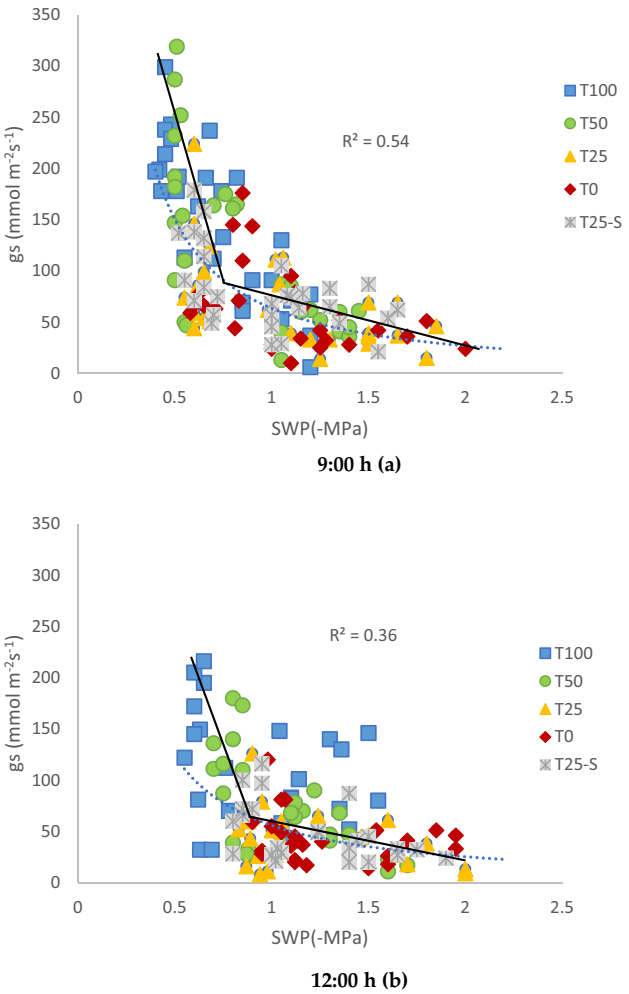

Fig. 3 Blue dotted line indicates the relationship between Stem Water Potential (SWP) and Stomatal conductance (gs) at 9:00 h (**a**) and at 12:00 h (**b**). Symbols represent the mean values for each irrigation treatment: T100 (reference treatment), T50 (50% of reference treatment), T25 (25% of reference treatment), T0 (rainfed), and T25-S (25% of reference treatment applied subsurface), over two years (2021 and 2022). The black line represents the piecewise linear regression (colour figure online)

The highest correlation for SWP was with TL (r = − 0.82) at 9:00 h (Fig. 5a). However, the highest correlation for SWP at 12:00 h was with Tc (r = − 0.75), Tc–Ta (r = − 0.72) and CWSIj (r = − 0.70). The SWP had significant correlations with TL and CWSIj at both times. As for gs, the highest correlations were with TL and TL–Ta at both times, ranging from r = − 0.70 to r = − 0.79.

In general, SWP showed a higher correlation with all indices at 12:00 h than at 9:00 h, except for TL and gsmodel(TL), which registered a higher correlation at 9:00 h, and CWSIj(TL), which showed no correlation at 12:00 h. Regarding gs, it was similar to SWP, showing a higher correlation with all indices at 12:00 h than at 9:00 h, except for TL–Ta, CWSIj(TL), and gsmodel(TL),

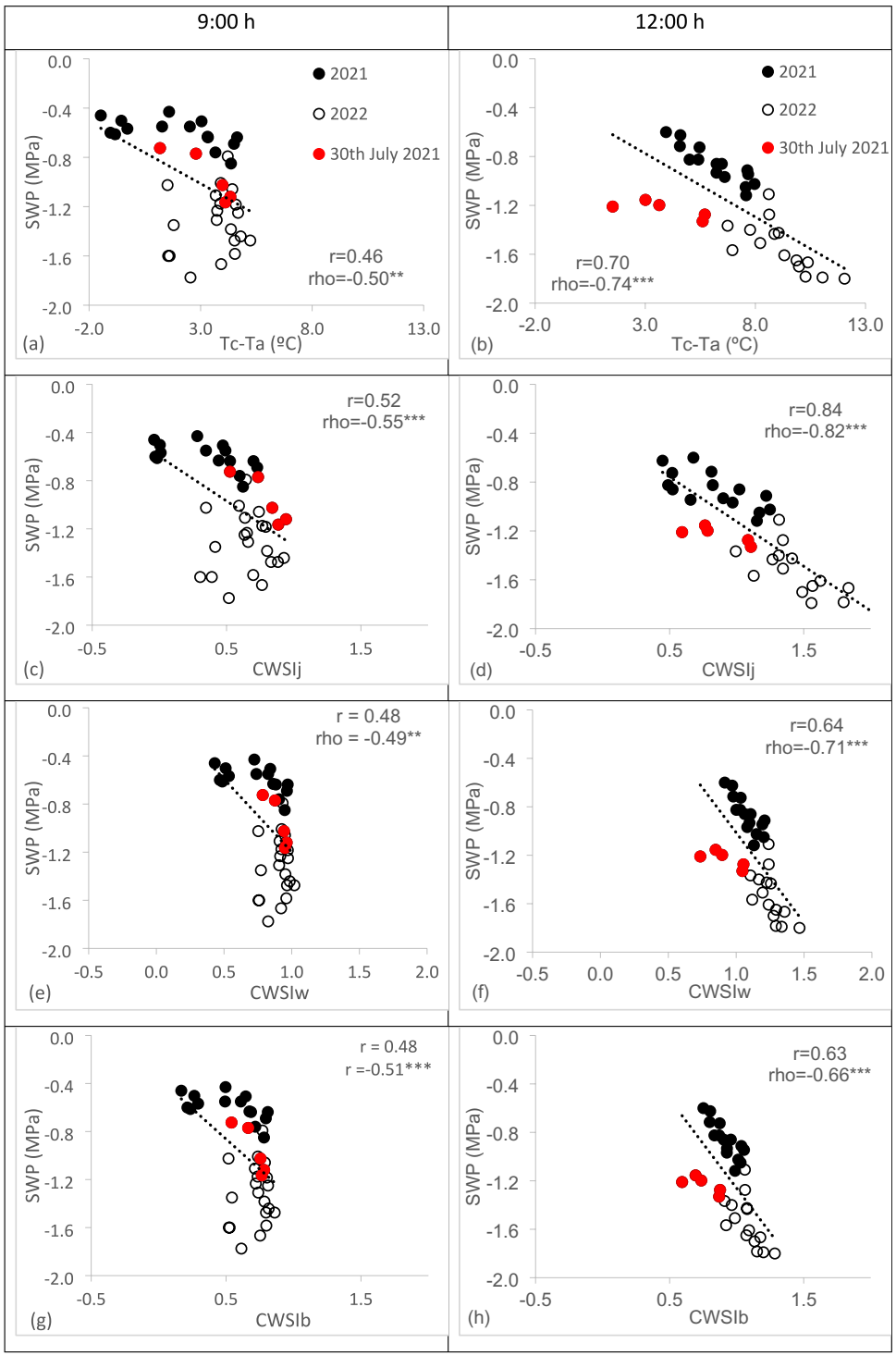

Fig. 4 Relationship between thermal indices (Tc-Ta, CWSIj, CWSIw, CWSIb) and Stem Water Potential (SWP) at 9:00 h (**a**, **c**, **e**, **g**) and 12:00 h (**b**, **d**, **f**, **h**) for measurement dates of 2021 (solid black circles) and measurement dates of 2022 (open black circles). The red solid circle corresponds to July 30 2021 values. The dotted line is the regression line. The rho coefficient indicates the result of a Spearman test (colour figure online)

where the correlations were higher at 9:00 h. Overall, results show that the thermal indices had higher correlations with SWP than with gs.

On the other hand, the correlation between gs and SWP was higher at 9:00 h (r = 0.69) than at 12:00 h (r = 0.47).

Discussion

The study was carried out during the irrigation period (June–August) when VPD was high, and the canopy was

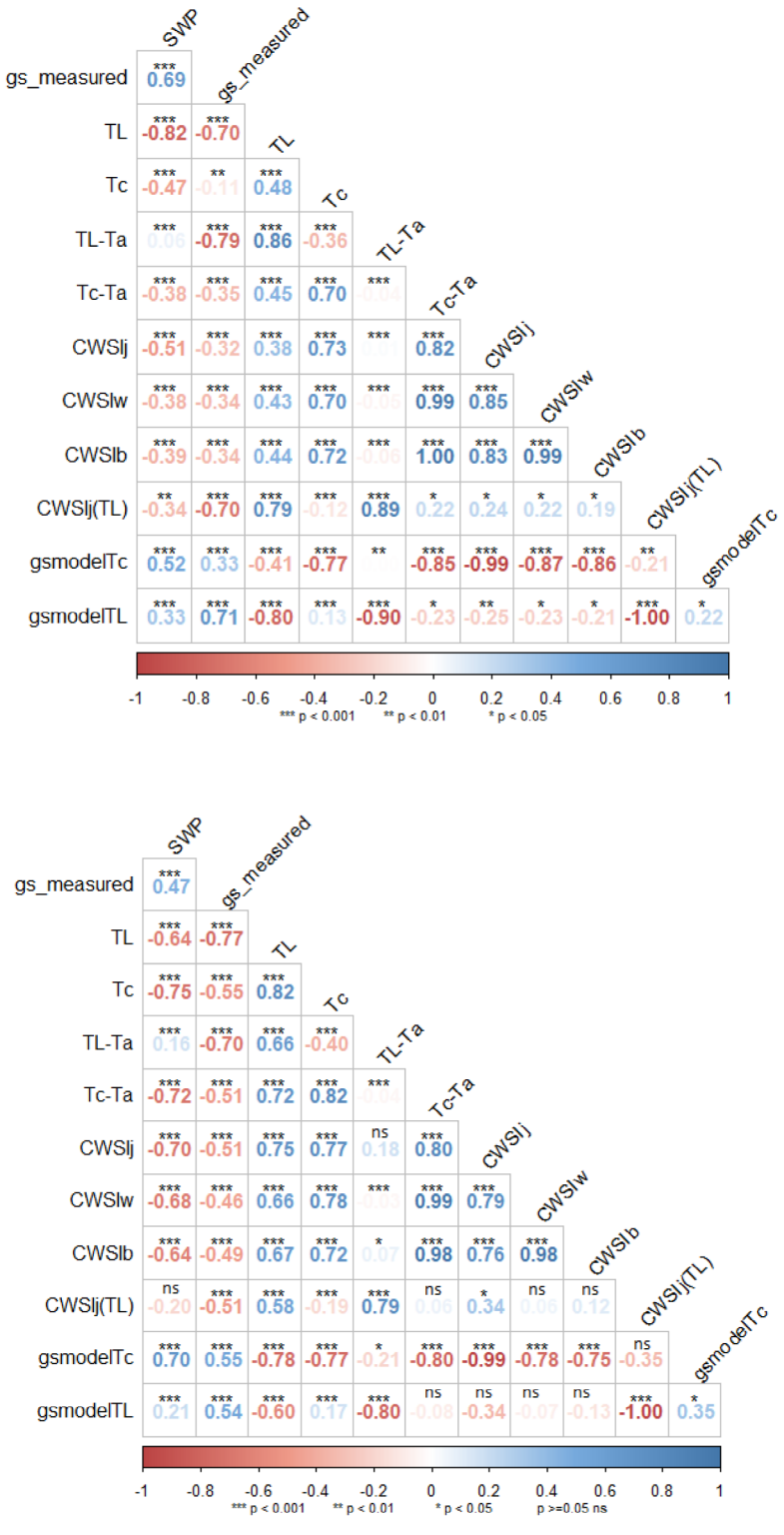

Fig. 5 Spearman correlation matrix for thermal indices and physiological parameters at 9:00 h (**a**) and 12:00 h (**b**) on the days of the UAS flight for the vines under irrigation treatments in the experimental vineyard (Toledo, Spain)

completely developed. We observed different relationships between SWP and the various versions of CWSI, which differ in the way that wet and dry edges are calculated (Fig. 4). The year of the study has a strong influence on the water status of the vines. The 2022 season was warmer than 2021, resulting in a maximum Tc–Ta (12.8°C) in the

vines in 2022 and severe water stress, with a minimum value of SWP (− 2 MPa). Under these conditions, the thermal indices were less sensitive to changes in SWP.

Although the SWP has certain limitations (García-Tejera et al. 2021; Nieto et al. 2022), this traditional agronomic assessment tool (Naor 2000; Choné et al. 2001; Girona et al. 2006) clearly identified the different irrigation treatments in our study. SWP is a parameter that integrates the water status of the plant with soil moisture conditions and atmospheric demand. Some studies contend that SWP can be influenced by canopy growth, which modifies the root to leaf area ratio and hence the hydraulic conductivity of the soil–plant-atmosphere continuum (Nieto et al. 2022; Garcia-Tejera et al. 2023). When there is a strong coupling between the canopy and the atmosphere, as there is in vineyards (Lu et al. 2003) both stomatal conductance and leaf area can exert great control over canopy-scale water loss (Tuzet et al. 2003; Zhang et al. 2012) fostering higher potential water vapor transfer to the atmosphere (Jarvis and McNaughton 1986). Wang et al. (2018) observed the influence of canopy height variations on aerodynamic resistances, subsequent cooling, and ultimately, canopy temperature. Therefore, it is necessary to consider vegetative development as a relevant factor in the energy exchange between the canopy and the atmosphere. In our study, it was observed that in the dry year (2022), there were no significant differences in the vegetative development of the canopy among the different irrigation treatments, which suggests that variations in Tc–Ta are not primarily due to changes in canopy development.

A general difficulty when evaluating remote sensing-based indicators with field data is the mismatch between spatial scales and the differences in the controls of processes at leaf and canopy levels. For example, at the leaf level, TL showed better correlations with SWP at 9:00 h than at 12:00 h, contrary to Tc (Fig. 5a,b). TL also showed good correlations with gs at both times (Fig. 5a, b). However, at solar noon, the correlation between TL and SWP was lower than the one between Tc and SWP. Gates (1964) and Jones (2002) both observed that TL was more susceptible to fluctuations in environmental conditions than Tc. This can be explained by the fact that leaf measurements do not adequately represent the whole plant water status (Turner 1990; Hernández-Montes et al. 2020), which is a common issue affecting experiments based on leaf-scale measurements (Nieto et al. 2022). Other factors influencing TL versus Tc differences could be related to the fact that the images contain more shade in the morning, which we did not fully account for in our corrections, as well as the higher error due to the use of the uncooled thermal camera compared to thermocouples (Bellvert et al. 2015).

The different approaches to estimate the dry and wet edges of the CWSI based on Tc reflects the whole plant water status. In our study, when the CWSI was estimated using TL (CWSIj (TL)) instead of Tc, it correlated better with the water status variable measured at the leaf level, gs; at 9:00 h (Fig. 5a), conversely, when CWSIj was estimated using Tc, it correlated better with SWP at 9:00 and 12:00 h (Fig. 5a,b).

An important finding was that solar noon was the best time to apply the CWSI as it better correlated with SWP and gs at 12:00 h than at 9:00 h in all approaches (Fig. 5b). In fact, it has been shown that the best time of the day for assessments of water stress based on Tc was 12:00 h (Ehrler et al. 1978). In our study, we observed that the range of SWP was lower in the morning due to the lower evaporative demand. Soil moisture does not change as much over the course of the day (Tuzet et al. 2003), therefore, the differences observed in the CWSI-SWP relationship between 9:00 h and 12:00 h were mainly due to the atmospheric conditions. There are clear differences in the atmospheric water vapor demand between solar noon and morning. The higher atmospheric water vapor demand (higher VPD) at solar noon would reduce SWP and induce stomatal closure, leading to increases in Tc–Ta. The atmospheric conditions at solar noon drive water gradients across the soil–plant water continuum, highlighting differences among water treatments.

Thus, for given micrometeorological conditions, Tc primarily depends on gs, the effect of which on transpiration rates is closely related to the water status of the plant (Jackson 1982) and climatic conditions. Tc is more similar among irrigation treatments in the morning, (Fig. 2g) than at solar noon (Fig. 2h), as plants transpire close to potential rates, and stomata are fully open. In the morning, the evaporative cooling demand is much lower. Additionally, in the morning, respiratory activity impacts the stomatal opening and closure, affecting the negative linear relationship between Tc and SWP (Gardner et al. 1981).

The results of our study show a clear year effect; in the warmer year (2022), SWP was markedly lower than in 2021. In 2022, the plants exhibited low anomalous SWP values at 9:00 h, similar to those observed at solar noon (Fig 2a, b). This indicated increased water stress during the 2022 season compared to 2021. The effect was observed in a change in the linear CWSI-SWP relationship, with stronger correlations at 12:00 h than at 9:00 h, as evidenced by the values of r and rho for all the thermal indices (Fig. 4b, d, f, and h). Other authors have observed this linear relationship (Yuan et al. 2004; Gonzalez-Dugo et al. 2013; Bellvert et al. 2014; Gutiérrez et al. 2021) however, it was less apparent at 12:00 h in 2021, especially for Tc–Ta (Fig. 4b). There was a specific date in 2021 (July 30 2021) when, at solar noon (Fig. 4b, d, f, g), SWP did not correlate well with Tc. On this day, the SWP was below what would be expected according to the linear relationship. However, despite the anomalous value of that date, CWSIj was the only thermal index that showed a closer relationship with SWP. The linear trend was

less consistent for the 9:00 h measurement in 2022, with rho values significant but lower than those for 12:00 h. It was observed that beyond a threshold value in SWP, the thermal indicators at 9:00 h tended to stabilize, becoming less sensitive to reductions in SWP (Fig. 4a, c, e, g).

The breakpoint in the correlation between gs and SWP (Fig. 3a) at 9:00 h occurred at − 0.57 MPa. This value marks a change in the dynamics between gs and SWP, which in turn affects the relationship between SWP and the thermal indices. In (Fig. 4 a, c, e and g), a certain stabilization is observed between − 0.5 and − 1 MPa for data corresponding to 2022 (the drier year), confirming the sensitivity of gs at lower SWP values (Sebastian et al. 2023). This breakpoint was particularly noticeable in the CWSIw and CWSIb indices (Fig. 4e, g). However, CWSIj and Tc–Ta showed greater dispersion under these conditions (Fig. 4a, c). This could be explained by their higher sensitivity to air temperature values. Our study used air temperature within the canopy (Ta), which might be affected by microclimatic changes (Jones 2002), instead of temperature at screen height (in our case, at a height of 2 m above the canopy).

Around − 0.57 MPa (Fig. 3a), stomatal closure was observed in the morning hours, showing a nonlinear relationship. This nonlinear relationship between SWP and gs has been observed in other crops, such as olive trees (Ben-Gal et al. 2009; Ahumada-Orellana et al. 2019) as well as in other studies of vineyards (Gutiérrez et al. 2021). It can be attributed to the effect of a very high VPD and evaporative demand (ETo) on transpiration rates and gs. This situation could have caused a high transpiration rate due to high vapor diffusivity and high gs, especially in the most irrigated treatment, reducing SWP and causing Tc and TL to be lower than expected for those SWP values. The CWSI (1-ET/ETp) is sensitive to changes in SWP even though the gs changes very little beyond the breakpoint in Fig. 3; therefore, SWP and gs may not necessarily result in the same vine response (Schlank et al. 2024). Under conditions of higher VPD and higher radiation, ET will exhibit a marginal increase but ETp will show a larger proportional increase, even if the gs remains almost constant. This will result in an increase in the CWSI (becoming drier) and a decrease in SWP. Although we might expect to observe better performance when gs is more responsive to SWP (before stomatal closure), we can nonetheless assume that in conditions of near stomatal closure, as in Fig. 3 after the breakpoint, ETp increases more than ET. This situation causes a higher CWSI, which is related to a reduction in SWP. Therefore, the CWSI may be sensitive to changes in SWP but not to gs.

Looking at the relationship between SWP and gs in the vines analyzed in this study, it is not entirely clear whether they are closer to isohydric or anisohydric behavior. Based on Bellvert et al. (2015) we applied the CWSIb, using the equation to obtain the baseline values, which include VPD and Tc–Ta corresponding to anisohydric behavior. However, isohydric and anisohydric behavior are on two ends of a continuum rather than being a binary classification. In other words, plants shift between strict regulation and looser regulation. This makes choosing a method to estimate stomatal regulation, as in Bellvert et al. (2015), a difficult task. For example, Zhang et al. (2012) observed a change from anisohydric behaviour under wet soil conditions to isohydric behaviour when soil water depleted over drying cycles. However, in our experiment, plants seemed to display more isohydric behavior in the morning (Fig. 3a) and more anisohydric behavior at solar noon (Fig. 3b). Other authors have observed similar transitions between anisohydric and isohydric behavior under water stress (Lovisolo et al. 2010; Tombesi et al. 2014; Martínez-Vilalta and Garcia-Forner 2017; Charrier et al. 2018; Levin et al. 2019; Gallo et al. 2022).

Depending on how much water is available, the plants show more anisohydric behaviour when irrigation is applied to fully replenish crop evapotranspiration, with loose stomatal control. As less water becomes available to the plants, the response shifts to more isohydric behavior, eventually reaching a point where irrigation is so restricted that the plants keep their stomata closed (Sebastian et al. 2023). This situation strengthens the relationship between CWSI and SWP at solar noon across water treatments, as plants are influenced by the soil–plant-atmosphere continuum (Fig. 4).

Similarly, Ben-Gal et al. (2009) observed that towards noon and early afternoon, the stomata of the stressed olive trees started closing after transpiring and losing water, resulting in an increase in canopy temperature. Therefore, in this case, the greater the stress, the larger the CWSI value, leading to a better assessment of water status in the trees.

The results obtained by Cifre et al. (2005) showed high dispersion in gs values when SWP was greater than− 2 MPa. Similar results were observed in olive by Marino et al. (2018), who suggested that a SWP–gs model for low-level stress (SWP > − 2 MPa) is not reliable. This dispersion at high SWP values is caused by the sensitivity of gs to other factors such as temperature, humidity, and incident irradiance (Jarvis 1976; Leuning 1995).

In this study, we have used CWSI as a proxy for SWP, although CWSI indicates the relationship between actual and potential evapotranspiration rates. For this reason, we also evaluated the gs derived from the Jackson model to assess the accuracy of CWSIj as a closer indicator of SWP. We compared the gs measured from the leaf with the gs estimated using Jackson's model fed with TL, which we denote gsmodel (TL), and with Tc, which we denote gsmodel(Tc) (Fig. 5a,b). When using the gsmodel(TL) instead of gsmodel(Tc), the correlations changes at 9:00 h (from r = 0.33 to r = 0.71) and 12:00 h (from r = 0.55 to r = 0.54). This indicates a reasonable performance by the

CWSI model, but suggests that there is a mismatch between the data used at one scale (drone—top of canopy leaves) and those from measurements at the leaf level. Additionally, to scale up from gs measured at the leaf level to gs at the canopy level, changes in Leaf Area Index(LAI) would have to be taken into account (Bu et al. 2021).

The robustness of the thermal-based indices depends on their ability to estimate the physiological parameter SWP across wide-ranging meteorological conditions or phenological state. Our findings confirm that simple thermal indictors such as Tc–Ta can identify varying levels of crop hydration using UAS temperature values (Tc), outperforming CWSIb or CWSIw at 12:00 h (Fig. 4b, f, h). However, these simple indicators are less accurate under extreme aridity, high VPD, and low SWP conditions, deviating from linear relationships. Conversely, ET-based stress indices calculated using high resolution imagery have shown a good relationship with water status in vineyard (Bellvert et al. 2020; Nieto et al. 2022; Burchard-Levine et al. 2024). CWSIj emerges as a suitable alternative from a climate change perspective—that is, under increasingly hot and arid conditions—with robust performance across different days and times (Fig. 4c, d), mainly due to the high resolution of the images that makes it possible to separate energy balance components from the vine canopy (Ortega-Farias et al. 2021; Ramírez-Cuesta et al. 2022). However, several parameters are needed to estimate the CWSIj, such as air and canopy temperatures, aerodynamic and canopy resistance, potential canopy resistance, canopy emissivity, incident solar radiation, and emitted radiation. Emerging or anticipated future technologies are expected to enable make it quicker to obtain accurate energy balance parameters. It is important to consider all the required meteorological parameters to develop methodologies or tools that enable crop monitoring under different climatic scenarios; ultimately, however, it will be up to the farmer to assess the potential of these indices and make decisions based on specific crop management needs.

Conclusions

This study underscores the effectiveness of thermal indices calculated data from sensors onboard UAS as a tool for estimating vineyard water status, thus enabling better irrigation management.

Our results confirmed that the best time for capturing thermal images from UAS is at 12:00 h solar time, when there is a closer relationship between thermal indices and SWP and a wider range of SWP and Tc values from vines under different irrigation treatments. The higher VPD at solar noon amplifies stomatal responses to the different soil moisture levels.

Regarding temperature as a whole plant indicator of water stress, our results confirmed the limitation of using TL based indices rather than Tc based indices to estimate SWP.

Among all the evaluated thermal indices, Tc–Ta and CWSIj were found to be the best at detecting variations in SWP within the vineyard across different times of day. The indicator Tc–Ta, calculated using UAS temperature values (Tc) and Ta from a portable weather station, had high precision at 12:00 h. However, in situations of severe water stress due to heat and aridity, this simple indicator did not work as well. Instead, CWSIj, which a stronger biophysical basis, emerged as a useful alternative, even though it requires the input of several parameters based on micrometeorological data.

Our study also showed changes in the behavior of Merlot from anisohydric to isohydric over the course of the day and the season. This finding supports the idea that plants' behavior in response to different stress levels and environmental conditions is not a categorical feature. As such, it limits the use of empirical models to estimate the wet and dry baselines (Tdry and Twet) as a function of VPD based on the isohydric/anisohydric categorization, as in CWSIb.

All around the world, reduced water availability poses a threat to the yield, quality, and economic viability of grapes grown for wine. Climate change projections point to warming and drying trends in the coming decades, jeopardizing the sustainability of viticulture. In this context, a significant research effort has been made in recent years to understand the effects of water stress on grapevine performance. Addressing these challenges in the future requires the development of a non-destructive, cost-effective, and easy-to-use method for continuously monitoring grapevine water status. The results obtained in this study can provide valuable information to guide the development of models for upscaling field measurements, thus enhancing our ability to manage irrigation more precisely and sustainably.

Supplementary Information The online version contains supplementary material available at https://doi.org/10.1007/s00271-024-00955-1.

Acknowledgements The authors thank Bodegas y Viñedos Casa del Valle for allowing us to work in their vineyards and the company UTW for supplying technical support and drone images.

Author contributions LKAP: conceptualization, fieldwork, methodology, data analysis, writing – original draft preparation- review & editing. MG: conceptualization, methodology, review, data analysis, editing. MGC: conceptualization, methodology, data analysis, review. AMT: conceptualization, methodology, data analysis, review.

Funding Open Access funding provided thanks to the CRUE-CSIC agreement with Springer Nature. Financial support was provided by Comunidad de Madrid through calls for grants to complete Doctorado Industrial IND2020/AMB-17341 and was greatly appreciated. M.G. was supported by a "María Zambrano" contract for the Universidad

Politécnica de Madrid, financed by the Spanish Ministerio de Universidades and by "European union NextGenerationEU/PRTR.

Data availability No datasets were generated or analysed during the current study.

Declarations

Conflict of interest Author Luz K. Atencia-Payares was employed by the company Unmanned Technical Works (UTW). The remaining authors declare that the research was conducted in the absence of any commercial or financial relationships that could be construed as a potential conflict of interest.

References

Ahumada-Orellana L, Ortega-Farías S, Poblete-Echeverría C, Searles PS (2019) Estimation of stomatal conductance and stem water potential threshold values for water stress in olive trees (cv. Arbequina). Irrig Sci 37:461–467. https://doi.org/10.1007/s00271-019-00623-9

Allen, R. G.; Hill; R.W.&Srikanth V (1994) Evapotranspiration parameters for variably-sied wetland. Am Soc Agric Eng Meet

Atencia Payares LK, Tarquis AM, Hermoso Peralo R et al (2023) Multispectral and thermal sensors onboard UAVs for heterogeneity in merlot vineyard detection: contribution to zoning maps. Remote Sens. https://doi.org/10.3390/rs15164024

Bellvert J, Zarco-Tejada PJ, Girona J, Fereres E (2014) Mapping crop water stress index in a 'pinot-noir' vineyard: comparing ground measurements with thermal remote sensing imagery from an unmanned aerial vehicle. Precis Agric 15:361–376. https://doi.org/10.1007/s11119-013-9334-5

Bellvert J, Marsal J, Girona J, Zarco-Tejada PJ (2015) Seasonal evolution of crop water stress index in grapevine varieties determined with high-resolution remote sensing thermal imagery. Irrig Sci 33:81–93. https://doi.org/10.1007/s00271-014-0456-y

Bellvert J, Marsal J, Girona J et al (2016) Airborne thermal imagery to detect the seasonal evolution of crop water status in peach, nectarine and saturn peach orchards. Remote Sens 8:1–17. https://doi.org/10.3390/rs8010039

Bellvert J, Jofre-Ĉekalović C, Pelechá A et al (2020) Feasibility of using the two-source energy balance model (TSEB) with sentinel-2 and sentinel-3 images to analyze the spatio-temporal variability of vine water status in a vineyard. Remote Sens. https://doi.org/10.3390/rs12142299

Ben-Gal A, Agam N, Alchanatis V et al (2009) Evaluating water stress in irrigated olives: correlation of soil water status, tree water status, and thermal imagery. Irrig Sci 27:367–376. https://doi.org/10.1007/s00271-009-0150-7

Berni JAJ, Zarco-Tejada PJ, Suárez L, Fereres E (2009) Thermal and narrowband multispectral remote sensing for vegetation monitoring from an unmanned aerial vehicle. IEEE Trans Geosci Remote Sens 47:722–738. https://doi.org/10.1109/TGRS.2008.2010457

Bota J, Tomás M, Flexas J et al (2016) Differences among grapevine cultivars in their stomatal behavior and water use efficiency under progressive water stress. Agric Water Manag 164:91–99. https://doi.org/10.1016/j.agwat.2015.07.016

Bu J, Gan G, Chen J et al (2021) Biophysical constraints on evapotranspiration partitioning for a conductance-based two source energy balance model. J Hydrol 603:127179. https://doi.org/10.1016/j.jhydrol.2021.127179

Burchard-Levine V, Borra-Serrano I, Peña JM et al (2024) Evaluating the precise grapevine water stress detection using unmanned aerial vehicles and evapotranspiration-based metrics. Irrig Sci. https://doi.org/10.1007/s00271-024-00931-9

Charrier G, Delzon S, Domec JC et al (2018) Drought will not leave your glass empty: low risk of hydraulic failure revealed by long-term drought observations in world's top wine regions. Sci Adv 4:1–10. https://doi.org/10.1126/sciadv.aao6969

Choné X, Van Leeuwen C, Dubourdieu D, Gaudillère JP (2001) Stem water potential is a sensitive indicator of grapevine water status. Ann Bot 87:477–483. https://doi.org/10.1006/anbo.2000.1361

Cifre J, Bota J, Escalona JM et al (2005) Physiological tools for irrigation scheduling in grapevine (Vitis vinifera L.): an open gate to improve water-use efficiency? Agric Ecosyst Environ 106:159–170. https://doi.org/10.1016/j.agee.2004.10.005

Clawson KL, Jackson RD, Pinter PJ (1989) Evaluating plant water stress with canopy temperature differences. Agron J 81:858–863. https://doi.org/10.2134/agronj1989.00021962008100060004x

Closas A, Molle F, Hernández-Mora N (2017) Sticks and carrots to manage groundwater over-abstraction in la mancha, Spain. Agric Water Manag 194:113–124. https://doi.org/10.1016/j.agwat.2017.08.024

Cohen Y, Alchanatis V, Meron M et al (2005) Estimation of leaf water potential by thermal imagery and spatial analysis. J Exp Bot 56:1843–1852. https://doi.org/10.1093/jxb/eri174

Cohen Y, Alchanatis V, Saranga Y et al (2017) Mapping water status based on aerial thermal imagery: comparison of methodologies for upscaling from a single leaf to commercial fields. Precis Agric 18:801–822. https://doi.org/10.1007/s11119-016-9484-3

Costa JM, Vaz M, Escalona J et al (2016) Modern viticulture in southern Europe: vulnerabilities and strategies for adaptation to water scarcity. Agric Water Manag 164:5–18. https://doi.org/10.1016/j.agwat.2015.08.021

Ehrler WL, Idso SB, Jackson RD, Reginato RJ (1978) Wheat canopy temperature: relation to plant water potential 1. Agron J 70:251–256. https://doi.org/10.2134/agronj1978.00021962007000020010x

FAO (2020) The state of food and agriculture 2020 overcoming water challenges in agriculture. Roma. https://doi.org/10.4060/cb1447en

Fuentes S, De Bei R, Tyerman SD (2013) New and emerging technologies for the vineyard: the vineyard of the future initiative. Wine Vitic J 28:38–45

Gallo AE, Perez Peña JE, González CV, Prieto JA (2022) Syrah and grenache (Vitis vinifera) revealed different strategies to cope with high temperature. Aust J Grape Wine Res 28:383–394. https://doi.org/10.1111/ajgw.12530

Garcia-Tejera O, Bonada M, Petrie PR et al (2023) Viticulture adaptation to global warming: modelling gas exchange, water status and leaf temperature to probe for practices manipulating water supply, canopy reflectance and radiation load. Agric for Meteorol 331:109351. https://doi.org/10.1016/j.agrformet.2023.109351

García-Tejera O, López-Bernal Á, Orgaz F et al (2021) The pitfalls of water potential for irrigation scheduling. Agric Water Manag. https://doi.org/10.1016/j.agwat.2020.106522

Gardner BR, Blad BL, Watts DG (1981) Plant and air temperatures in differentially-irrigated corn. Agric Meteorol 25:207–217. https://doi.org/10.1016/0002-1571(81)90073-X

Gates DM (1964) Leaf temperature and transpiration 1. Agron J 56:273–277. https://doi.org/10.2134/agronj1964.00021962005600030007x

Girona J, Mata M, Del Campo J et al (2006) The use of midday leaf water potential for scheduling deficit irrigation in vineyards. Irrig Sci 24:115–127. https://doi.org/10.1007/s00271-005-0015-7

Gonzalez-Dugo V, Zarco-Tejada P, Nicolás E et al (2013) Using high resolution UAV thermal imagery to assess the variability in the water status of five fruit tree species within a commercial orchard. Precis Agric 14:660–678. https://doi.org/10.1007/s11119-013-9322-9

Gonzalez-Dugo V, Zarco-Tejada PJ, Fereres E (2014) Applicability and limitations of using the crop water stress index as an indicator of water deficits in citrus orchards. Agric for Meteorol 198–199:94–104. https://doi.org/10.1016/j.agrformet.2014.08.003

Gutiérrez S, Fernández-Novales J, Diago MP et al (2021) Assessing and mapping vineyard water status using a ground mobile thermal imaging platform. Irrig Sci 39:457–468. https://doi.org/10.1007/s00271-021-00735-1

Hernández-Montes E, Escalona JM, Tomàs M, Medrano H (2020) Plant water status and genotype affect fruit respiration in grapevines. Physiol Plant 169:544–554. https://doi.org/10.1111/ppl.13093

Hsiao.T.C (1990) Measurement of plant water status. Agronomy No.30:243–279

Idso SB (1982) Non-water-stressed baselines: a key to measuring and interpreting plant water stress. Agric Meteorol 27:59–70. https://doi.org/10.1016/0002-1571(82)90020-6

Intrigliolo DS, Castel JR (2010) Response of grapevine cv. "tempranillo" to timing and amount of irrigation: water relations, vine growth, yield and berry and wine composition. Irrig Sci 28:113–125. https://doi.org/10.1007/s00271-009-0164-1

Irmak S, Haman DZ, Bastug R (2000) Determination of crop water stress index for irrigation timing and yield estimation of corn. Agron J 92:1221–1227. https://doi.org/10.2134/agronj2000.9261221x

Jackson RD, Reginato RJ, Idso SB (1977) Wheat canopy temperature: a practical tool for evaluating water requirements. Water Resour Res 13:651–656. https://doi.org/10.1029/WR013i003p00651

Jackson RD, Idso SB, Reginato RJ, Pinter PJ (1981) Canopy temperature as a crop water stress indicator. Water Resour Res 17:1133–1138. https://doi.org/10.1029/WR017i004p01133

Jackson RD (1982) Canopy Temperature and Crop Water Stress. ACADEMIC PRESS, INC.

Jarvis PG (1976) The interpretation of the variations in leaf water potential and stomatal conductance found in canopies in the field. Philos Trans R Soc London B Biol Sci 273:593–610. https://doi.org/10.1098/rstb.1976.0035

Jarvis PG, McNaughton KG (1986) Stomatal Control of Transpiration: Scaling Up from Leaf to Region pp 1–49

Jones HG (1999) Use of infrared thermometry for estimation of stomatal conductance as a possible aid to irrigation scheduling. Agric for Meteorol 95:139–149. https://doi.org/10.1016/S0168-1923(99)00030-1

Jones HG (2002) Use of infrared thermography for monitoring stomatal closure in the field: application to grapevine. J Exp Bot 53:2249–2260. https://doi.org/10.1093/jxb/erf083

Jones HG, Corlett JE (1992) Current topics in drought physiology. J Agric Sci 119:291–296. https://doi.org/10.1017/S0021859600012144

Jones HG, Serraj R, Loveys BR et al (2009) Thermal infrared imaging of crop canopies for the remote diagnosis and quantification of plant responses to water stress in the field. Funct Plant Biol 36:978–989. https://doi.org/10.1071/FP09123

Jones HG (2004) Application of Thermal Imaging and Infrared Sensing in Plant Physiology and Ecophysiology. pp 107–163

Leeuwen C Van, Tregoat O, Choné X, et al (2009) Vine water status is a key factor in grape ripening and vintage quality for red bordeaux wine. How can it be assessed for vineyard management purposes? J Int des Sci la Vigne du Vin 43:121–134. https://doi.org/10.20870/oeno-one.2009.43.3.798

Leinonen I, Jones HG (2004) Combining thermal and visible imagery for estimating canopy temperature and identifying plant stress. J Exp Bot 55:1423–1431. https://doi.org/10.1093/jxb/erh146

Leuning R (1995) A critical appraisal of combine stomatal model C3 plants. Plant Cell Environ 18:339–355

Levin AD, Williams LE, Matthews MA (2019) A continuum of stomatal responses to water deficits among 17 wine grape cultivars (Vitis vinifera). Funct Plant Biol 47:11–25. https://doi.org/10.1071/FP19073

Lovisolo C, Perrone I, Carra A et al (2010) Drought-induced changes in development and function of grapevine (Vitis spp.) organs and in their hydraulic and non-hydraulic interactions at the whole-plant level: a physiological and molecular update. Funct Plant Biol. https://doi.org/10.1071/FP09191

Lu P, Yunusa IAM, Walker RR, Müller WJ (2003) Regulation of canopy conductance and transpiration and their modelling in irrigated grapevines. Funct Plant Biol 30:689. https://doi.org/10.1071/FP02181

Maes WH, Steppe K (2012) Estimating evapotranspiration and drought stress with ground-based thermal remote sensing in agriculture: a review. J Exp Bot 63:4671–4712. https://doi.org/10.1093/jxb/ers165

Marino G, Caruso T, Ferguson L, Marra FP (2018) Gas exchanges and stem water potential define stress thresholds for efficient irrigation management in olive (Olea europea L.). Water 10:342. https://doi.org/10.3390/w10030342

Martínez-Vilalta J, Garcia-Forner N (2017) Water potential regulation, stomatal behaviour and hydraulic transport under drought: deconstructing the iso/anisohydric concept. Plant Cell Environ 40:962–976. https://doi.org/10.1111/pce.12846

Meron M, Tsipris J, Orlov V et al (2010) Crop water stress mapping for site-specific irrigation by thermal imagery and artificial reference surfaces. Precis Agric 11:148–162. https://doi.org/10.1007/s11119-009-9153-x

Meron MTJCD (2003) Remote mapping of crop water status to assess spatial variability of crop stress. Precis Agric 405–410

Ministerio de Agricultura P y A (MAPA) (2021) Estadisticas Agrarias. In: ttps://www.mapa.gob.es/estadistica/pags/anuario/2021/CAPITULOS PDF/AE21-C07.pdf. Spain

Möller M, Alchanatis V, Cohen Y et al (2007) Use of thermal and visible imagery for estimating crop water status of irrigated grapevine. J Exp Bot 58:827–838. https://doi.org/10.1093/jxb/erl115

Moyano MC, Garcia M, Palacios-Orueta A et al (2018) Vegetation water use based on a thermal and optical remote sensing model in the mediterranean region of doñana. Remote Sens. https://doi.org/10.3390/rs10071105

Naor A (2000) Midday stem water potential as a plant water stress indicator for irrigation scheduling in fruit trees. Acta Hortic. https://doi.org/10.17660/ActaHortic.2000.537.52

Nieto H, Alsina MM, Kustas WP et al (2022) Evaluating different metrics from the thermal-based two-source energy balance model for monitoring grapevine water stress. Irrig Sci 40:697–713. https://doi.org/10.1007/s00271-022-00790-2

Ortega-Farias S, Esteban-Condori W, Riveros-Burgos C et al (2021) Evaluation of a two-source patch model to estimate vineyard energy balance using high-resolution thermal images acquired by

an unmanned aerial vehicle (UAV). Agric For Meteorol. https://doi.org/10.1016/j.agrformet.2021.108433
Pou A, Medrano H, Tomàs M et al (2012) Anisohydric behaviour in grapevines results in better performance under moderate water stress and recovery than isohydric behaviour. Plant Soil 359:335–349. https://doi.org/10.1007/s11104-012-1206-7
Ramírez-Cuesta JM, Consoli S, Longo D et al (2022) Influence of short-term surface temperature dynamics on treeorchards energy balance fluxes. Precision Agric 23:1394–1412. https://doi.org/10.1007/s11119-022-09891-6
Rejeb A, Abdollahi A, Rejeb K, Treiblmaier H (2022) Drones in agriculture: a review and bibliometric analysis. Comput Electron Agric 198:107017. https://doi.org/10.1016/j.compag.2022.107017
Romero M, Luo Y, Su B, Fuentes S (2018) Vineyard water status estimation using multispectral imagery from an UAV platform and machine learning algorithms for irrigation scheduling management. Comput Electron Agric 147:109–117. https://doi.org/10.1016/j.compag.2018.02.013
Santesteban LG, Di Gennaro SF, Herrero-Langreo A et al (2017) High-resolution UAV-based thermal imaging to estimate the instantaneous and seasonal variability of plant water status within a vineyard. Agric Water Manag 183:49–59. https://doi.org/10.1016/j.agwat.2016.08.026
Schlank R, Kidman CM, Gautam D et al (2024) Data-driven irrigation scheduling increases the crop water use efficiency of cabernet sauvignon grapevines. Irrig Sci 42:29–44. https://doi.org/10.1007/s00271-023-00866-7
Scholander PF, Bradstreet ED, Hemmingsen EA, Hammel HT (1965) Sap pressure in vascular plants. Science. https://doi.org/10.1126/science.148.3668.339
Schymanski SJ, Or D, Zwieniecki M (2013) Stomatal control and leaf thermal and hydraulic capacitances under rapid environmental fluctuations. PLoS One. https://doi.org/10.1371/journal.pone.0054231
Sebastian V, Nicolas O, Alvaro G, Samuel OF (2023) Effect of irrigation management on the relationship between stomatal conductance and stem water potential on cv. BIO Web Conf, Cabernet Sauvignon. https://doi.org/10.1051/bioconf/20235601012
Shackel KA, Ahmadi H, Biasi W et al (1997) Plant water status as an index of irrigation need in deciduous fruit trees. HortTechnology 7:23–29
Tombesi S, Nardini A, Farinelli D, Palliotti A (2014) Relationships between stomatal behavior, xylem vulnerability to cavitation and leaf water relations in two cultivars of Vitis vinifera. Physiol Plant 152:453–464. https://doi.org/10.1111/ppl.12180
Toro G, Flexas J, Escalona JM (2019) Contrasting leaf porometer and infra-red gas analyser methodologies: an old paradigm about the stomatal conductance measurement. Theor Exp Plant Physiol 31:483–492. https://doi.org/10.1007/s40626-019-00161-x
Turner NC (1990) Plant water relations and irrigation management. Agric Water Manag 17:59–73. https://doi.org/10.1016/0378-3774(90)90056-5
Tuzet A, Perrier A, Leuning R (2003) A coupled model of stomatal conductance and photosynthesis for winter wheat. Photosynthetica 46:637–640. https://doi.org/10.1007/s11099-008-0110-0
Van Leeuwen C, Roby JP, De Rességuier L (2018) Soil-related terroir factors: a review. Oeno One. https://doi.org/10.20870/oeno-one.2018.52.2.2208
Vlassova L, Perez-Cabello F, Nieto H et al (2014) Assessment of methods for land surface temperature retrieval from landsat-5 TM images applicable to multiscale tree-grass ecosystem modeling. Remote Sens 6:4345–4368. https://doi.org/10.3390/rs6054345
Wang S, Garcia M, Bauer-Gottwein P et al (2019) High spatial resolution monitoring land surface energy, water and CO2 fluxes from an unmanned aerial system. Remote Sens Environ 229:14–31. https://doi.org/10.1016/j.rse.2019.03.040
Wang S, Garcia M, Ibrom A et al (2018) Mapping root-zone soil moisture using a temperature-vegetation triangle approach with an unmanned aerial system: Incorporating surface roughness from structure from motion. Remote Sens. https://doi.org/10.3390/rs10121978
Wheaton AD, Cooley NC, Dunn GM, et al (2011) Use of thermal imagery to detect water stress during berry ripening in vitis vinifera l. "cabernet sauvignon." Acta Hortic. https://doi.org/10.17660/ActaHortic.2011.889.12
Williams LE, Baeza P (2007) Relationships among ambient temperature and vapor pressure deficit and leaf and stem water potentials of fully irrigated, field-grown grapevines. Am J Enol Vitic 58:173–181. https://doi.org/10.5344/ajev.2007.58.2.173
Yuan G, Luo Y, Sun X, Tang D (2004) Evaluation of a crop water stress index for detecting water stress in winter wheat in the north China plain. Agric Water Manag 64:29–40. https://doi.org/10.1016/S0378-3774(03)00193-8
Zhang Y, Oren R, Kang S, Niinemets Ü (2012) Spatiotemporal variation of crown-scale stomatal conductance in an arid Vitis vinifera L. cv. merlot vineyard: direct effects of hydraulic properties and indirect effects of canopy leaf area. Tree Physiol 32:262–279. https://doi.org/10.1093/treephys/tpr120